NUREG/CR-1791
ORNL/NUREG/TM-417
Dist. Category R7

Contract No. W-7405-eng-26

Engineering Technology Division

LMFBR AEROSOL RELEASE AND TRANSPORT PROGRAM QUARTERLY PROGRESS REPORT FOR APRIL–JUNE 1980

T. S. Kress M. L. Tobias

Manuscript Completed – November 26, 1980
Date Published – December 1980

Prepared for the
U.S. Nuclear Regulatory Commission
Office of Nuclear Regulatory Research
Under Interagency Agreements DOE 40-551-75 and 40-552-75

NRC FIN No. B0121

Prepared by the
OAK RIDGE NATIONAL LABORATORY
Oak Ridge, Tennessee 37830
operated by
UNION CARBIDE CORPORATION
for the
DEPARTMENT OF ENERGY

CONTENTS

	Page
FOREWORD	v
SUMMARY	vii
GLOSSARY OF ACRONYMS	ix
ABSTRACT	1
1. INTRODUCTION	1
2. EXPERIMENTAL PROGRAM	3
2.1 Source Term and SIMMER Verification Experiments in FAST/CRI-III	3
2.1.1 Introduction	3
2.1.2 Discussion of results from FAST underwater tests	3
2.1.3 Discussion of results from CRI-III tests	7
2.2 Secondary Containment Aerosol Studies in NSPP	15
2.2.1 Introduction	15
2.2.2 Uranium oxide aerosol test No. 208	15
2.2.3 Sodium oxide aerosol test No. 108	17
2.3 Basic Aerosol Experiments in CRI-II	19
2.3.1 Introduction	19
2.3.2 Comparison of size measurements performed by means of the spiral centrifuge with various impactors	19
2.3.3 Intercomparison of aerosol size test data with other laboratories	22
3. ANALYTICAL PROGRAM	27
3.1 Improved Formulas for Bubble-Liquid Interface Temperatures for FAST Experiment Analysis	27
3.2 Programming Efforts in Support of the NSPP Experimental Program	28
REFERENCES	29

FOREWORD

This report summarizes progress under the Aerosol Release and Transport (ART) Program [sponsored by the Division of Reactor Safety Research of the Nuclear Regulatory Commission (NRC)] for the period April–June 1980.

Work on this program was initially reported as Volume III of a four-volume series entitled *Quarterly Progress Report on Reactor Safety Programs Sponsored by the NRC Division of Reactor Safety Research*. Prior reports of this series are

Report No.	Period covered
ORNL/TM-4655	April–June 1974
ORNL/TM-4729	July–September 1974
ORNL/TM-4805	October–December 1974
ORNL/TM-4914	January–March 1975
ORNL/TM-5021	April–June 1975

Beginning with the report covering the period July–September 1975, work under this program is now being reported as *LMFBR Aerosol Release and Transport Program Quarterly Progress Report*. Prior reports under this title are

Report No.	Period covered
ORNL/NUREG/TM-8	July–September 1975
ORNL/NUREG/TM-9	October–December 1975
ORNL/NUREG/TM-35	January–March 1976
ORNL/NUREG/TM-59	April–June 1976
ORNL/NUREG/TM-75	July–September 1976
ORNL/NUREG/TM-90	October–December 1976
ORNL/NUREG/TM-113	January–March 1977
ORNL/NUREG/TM-142	April–June 1977
ORNL/NUREG/TM-173	July–September 1977
ORNL/NUREG/TM-193	October–December 1977
ORNL/NUREG/TM-213	January–March 1978
ORNL/NUREG/TM-244	April–June 1978
ORNL/NUREG/TM-276	July–September 1978
ORNL/NUREG/TM-318	October–December 1978
ORNL/NUREG/TM-329	January–March 1979
ORNL/NUREG/TM-354	April–June 1979
ORNL/NUREG/TM-376	July–September 1979
ORNL/NUREG/TM-391	October–December 1979
ORNL/NUREG/TM-416	January–March 1980

Copies of all these reports are available from the Technical Information Center, Oak Ridge, Tennessee 37830.

SUMMARY

M. L. Tobias

The Aerosol Release and Transport (ART) Program at Oak Ridge National Laboratory (ORNL) is designed to investigate the release, transport, and behavior of radionuclides originating from a severe accident resulting in core melting. The experimental program is being conducted in the Fuel Aerosol Simulant Test (FAST) Facility [which also includes the Containment Research Installation-III (CRI-III) vessel], the Nuclear Safety Pilot Plant (NSPP) Facility, and the CRI-II Facility. The analytical effort is designed to support the experiments and to provide an independent assessment of the safety margins that exist for the assessment of the radiological consequences of a core meltdown accident.

During this period, 13 tests were performed in the FAST/CRI-III facility, including 8 underwater tests in the FAST facility and 5 tests in the CRI-III facility. In the underwater tests, pressure pulses were recorded for at least 100 ms after capacitor discharge and high speed movies were taken. In addition, pressure changes were recorded in the argon cover gas, and acoustic "pulse echo" measurements were made in attempts to monitor bubble motion. Uranium oxide was found in the cover gas only in the single hot water (359 K) test. This test also showed a small secondary pressure event in the argon cover gas that may be due to bubble re-expansion after first collapse.

One of the five CRI-III tests was of the "energy density" type while the remainder were related to the Sandia Normalization test series. A new viewing system technique for temperature measurements appeared to work well during the preheat and capacitor discharge stages of the experiments. In addition to these tests, three earlier preheat-only tests are discussed. Photographs of cross-section cuts were made, and the phase change and void formation patterns are described in relation to the experimental conditions which produced them.

In the NSPP facility, a uranium oxide test was performed under wet conditions and a low concentration sodium oxide aerosol test was done under dry conditions. The most noticeable effect of moisture in the uranium oxide test was a change in the physical appearance of the aerosol particles from the usual chain-like appearance to that of nearly spherical agglomerates. Despite this change, settling rates did not appear to be much different from those for dry aerosols. Data for aerosol diameter and concentrations as functions of time are presented. In the sodium test, the mass concentration reached 2.25 $\mu g/cm^3$. Aerosol concentrations fell off more slowly than for previous tests in the 6 to 25 $\mu g/cm^3$ range; cascade impactor results for the diameter were not much different, however.

As part of the basic aerosol experimental program, a comparative review of aerosol size measurements performed by the spiral centrifuge with those made by other methods is under way, and some of the results are discussed. Generally, it is found that while low-velocity commercial size-measuring instruments can give good qualitative size distributions, the centrifuge instrument gives more precise measurement.

In the analytical program, two formulas for bubble-liquid interface temperatures were developed based on the exact solution in slab geometry.

These give better results than those developed from the integral balance method reported earlier. In another area, programming improvements have been made to make the computer processing of NSPP data more efficient.

GLOSSARY OF ACRONYMS

ART	Aerosol Release and Transport
ACRR	Annular Core Research Reactor
AMMD	aerodynamic mass median diameter
CDA	core-disruptive accident
CDV	capacitor discharge vaporization
CRI	Containment Research Installation
CSTF	Containment Systems Test Facility
FAST	Fuel Aerosol Simulant Test
GSD	geometric standard deviation
HCDA	hypothetical core-disruptive accident
LASL	Los Alamos Scientific Laboratory
LMFBR	Liquid-Metal Fast Breeder Reactor
NRC	Nuclear Regulatory Commission
NSPP	Nuclear Safety Pilot Plant
ORNL	Oak Ridge National Laboratory
PSL	polystyrene latex
PT	plasma torch
SEM	scanning electron microscope
TEM	transmission electron microscope

LMFBR AEROSOL RELEASE AND TRANSPORT PROGRAM QUARTERLY PROGRESS REPORT FOR APRIL–JUNE 1980

T. S. Kress M. L. Tobias

ABSTRACT

This report summarizes progress for the Aerosol Release and Transport (ART) Program sponsored by the Division of Reactor Safety Research of the Nuclear Regulatory Commission for the period April–June 1980. Topics discussed include (1) recent capacitor discharge vaporization (CDV) underwater tests conducted in the Fuel Aerosol Simulant Test (FAST) Facility to evaluate the disassembly process, including bubble dynamics and UO_2 vapor condensation and transport; (2) tests in the Containment Research Installation-III (CRI-III) vessel to evaluate UO_2 temperatures during melting and CDV discharge; (3) a single-component U_3O_8 aerosol experiment under moist conditions and a dry sodium oxide aerosol experiment in the Nuclear Safety Pilot Plant (NSPP); (4) comparisons using the Los Alamos Scientific Laboratory–Stöber spiral centrifuge with other experimental techniques; and (5) new formulas for bubble-liquid interface temperatures for FAST experiment analysis.

Keywords: aerosol, core meltdown hypothetical accident, LMFBR fission product release, fission product transport, ex-reactor experiment, safety, radionuclide transfer.

---

1. INTRODUCTION

The Aerosol Release and Transport (ART) Program at Oak Ridge National Laboratory (ORNL), sponsored by the Division of Reactor Safety Research of the Nuclear Regulatory Commission (NRC), is a safety program concerned with radionuclide release and transport. Its scope includes radionuclide release from fuel, transport to and release from primary containment boundaries, and behavior within containments. The overall goal of the program is to provide the analytical methods and experimental data necessary to assess the quantity and transient behavior of radionuclides released from reactor cores as a result of postulated events of varying severity up to and including accidents resulting in core melting.

The program is divided into several related experimental and analytical activities as summarized below:

1. development of a capacitor discharge vaporization (CDV) system for deposition of energy in simulated LMFBR fuel (UO_2) that will provide a nonnuclear means for studying the fuel reponse to energy depositions characteristic of severe accident conditions;

2. study of fuel interactions, expansion, and thermal behavior within the sodium pool as the resultant fuel-vapor bubble is produced and transported through the sodium to the cover-gas region;
3. development of alternative means for generating fuel-simulant aerosols on a relatively continuous basis;
4. study of the characteristics and behavior of fuel-simulant aerosols in several small vessels; and
5. production and study of fuel-simulant and sodium aerosols in the Nuclear Safety Pilot Plant (NSPP) for the validation of models, with particular emphasis on the behavior of mixtures of the two nuclear aerosol species.

Varying levels of effort are anticipated within these categories, with analytical models accompanying the experimental work. The analytical requirements fall into three categories: (1) fuel response to high rates of energy deposition, (2) fuel-bubble dynamic behavior and transport characteristics under sodium, and (3) dynamic aerosol behavior at high concentrations in the bubble and containment atmospheres.

An attempt will be made to consolidate the analyses and data and to present them in a manner that will facilitate direct assessment of the radiological hazard associated with arbitrary hypothetical accident scenarios.

2. EXPERIMENTAL PROGRAM

2.1 Source Term and SIMMER Verification Experiments in FAST/CRI-III

A. L. Wright A. M. Smith
J. M. Rochelle

2.1.1 Introduction

The Fuel Aerosol Simulant Tests (FAST) and the Containment Research Installation-III (CRI-III) tests are performed by using the CDV technique to place uranium dioxide fuel samples into the high energy states that could be produced in severe reactor accidents. The primary goals of the FAST/CRI-III test program are to (1) use the experimental results as a base for developing analytical models that could then be used to predict fuel transport through the coolant in case of an accident and (2) perform experiments in support of the program to verify models in the Los Alamos Scientific Laboratory (LASL) SIMMER computer code.

During this quarter, 13 tests were performed in the FAST/CRI-III Facility, including 8 underwater tests in the FAST Facility and 5 tests in the CRI-III Facility. Test specimen and electrical energy input data are presented in Tables 1 and 2. Individual test results and conclusions are presented in Sects. 2.1.2 and 2.1.3. In addition, results from CDV 97 and 98 (performed last quarter) are presented in Sect. 2.1.3.

2.1.2 Discussion of results from FAST underwater tests

Eight underwater tests were performed in the FAST Facility this quarter. A number of these were performed at conditions outlined in the FAST experimental plan.[1] For all of these tests, the argon cover gas pressure was slightly greater than 0.101 MPa. Parameters varied in the tests were the xenon gas pressure in the test sample, the water temperature, and the water height above the test sample. A summary of the pressure, temperature, and water height settings is presented in Table 3.

In each test the pressure pulses produced by bubble expansion and contraction were measured. This was done using a Kaman Sciences pressure transducer that was mounted ~230 mm from the test sample; pressure signals were recorded for $\geq$100 ms after capacitor discharge. High-speed movies were taken of all tests. In addition to the movies, other techniques were used to "track" the bubbles formed; these included measurements of pressure changes in the argon cover gas and also acoustic "pulse-echo" measurements. Finally, a few minutes after capacitor discharge, the argon gas above the water was sampled to determine if any fuel vapor or aerosol had been transported through the water during the tests.

FAST 50. This was the second FAST test in which the xenon gas pressure inside the sample was maintained at a very small level (~27 μm Hg). CDV energy input was high, but steel tube rupture was poor, as in the previous test of this type, FAST 48. The presence of larger amounts of xenon gas in the sample may be enhancing steel tube breakup. No UO_2 aerosol was found in the cover gas after the test.

Table 1. Sample data

Test	Pellet stack mass (g)	Pellet stack length (mm)	Microsphere mass (g)	Quartz tube ID (mm)	Dimensions OD (mm)
FAST 50	17.49	89.9	33.08	9.72	17.17
FAST 51	17.30	89.3	32.33	9.70	17.14
FAST 52	17.46	89.7	33.62	9.70	17.56
FAST 53	17.36	90.2	32.75	9.70	16.76
FAST 54	17.30	89.9	33.09	9.70	16.83
FAST 55	17.48	89.9	32.06	9.70	17.20
FAST 56	17.31	89.9	33.69	9.70	16.55
FAST 57	17.66	91.8	32.17	9.70	16.65
CDV 101	17.50	90.0	32.74	9.70	17.20
CDV 102	17.35	90.2	32.36	9.72	17.68
CDV 103	21.29	110.9	32.85	9.73	17.05
CDV 104	21.35	111.0	38.42	9.73	16.93
CDV 105	21.47	111.9	39.27	9.73	16.76

Table 2. Preheat and capacitor discharge data[a]

Test	High preheat power (W)	Sample resistance after high preheat (Ω)	CDV time to arcing (ms)	CDV energy input to arcing (kJ)
FAST 50	1700	0.43	2.65	29.9
FAST 51	1700	0.50	2.45	25.0
FAST 52	1700	0.54	2.91	26.6
FAST 53	1700	0.43	1.44	15.6
FAST 54	1700	0.48	2.72	29.0
FAST 55	1700	0.44	2.39	27.3
FAST 56	1700	0.50	2.99	30.4
FAST 57	1700	0.46	2.02	21.8
CDV 101	2100	0.35	0.36	4.5
CDV 102	1700	0.43	1.61	20.4
CDV 103	2200	0.44	3.88	41.9
CDV 104	2200	0.45	2.30	26.4
CDV 105	2200	0.45	[b]	[b]

[a] No capacitor discharge was performed in CDV 105. In all other tests, four capcitor banks were charged to ~1950 V (75 kJ).

[b] No capacitor discharge.

Table 3. Pressure, temperature, and liquid height conditions for FAST underwater tests 50 through 57

Test	Argon gas pressure[a] (MPa)	Xenon gas pressure[b] (MPa)	Water temperature (K)	Water height[c] (mm)
FAST 50	0.122	~0	298	1120
FAST 51	0.123	0.513	298	710
FAST 52	0.122	0.520	298	710
FAST 53	0.122	0.513	298	710
FAST 54	0.122	0.101	298	710
FAST 55	0.122	0.513	298	1120
FAST 56	0.122	0.513	359	1120
FAST 57	0.122	0.513	298	1120

[a] This refers to the argon gas space above the water.

[b] Xenon gas is inserted into the UO_2 test sample; after capacitor discharge, the xenon becomes part of the bubble produced.

[c] This refers to the water height above the level of the test sample.

FAST 51. This test was done with the water height reduced to 710 mm. CDV energy input was not large, and steel tube (surrounding the fuel sample) rupture was poor. The first bubble oscillation period (the time between the pressure pulse caused by bubble formation and the pulse caused by bubble collapse and re-expansion) was about 10 ms less than in tests where the water height was 1120 mm. Even though the water height was reduced, no UO_2 aerosol was found in the cover gas. We attempted to measure the argon gas pressure change caused by bubble formation, but, compared to tests where the water height was 1120 mm, the cover gas volume was so large that the pressure change caused by bubble expansion was too small to measure.

FAST 52. The water height was again 710 mm for this test. Though CDV energy input was higher than in CDV 51, steel tube rupture was again poor. Results were essentially the same as in FAST 51.

FAST 53. Test conditions were the same as for FAST 51 and 52. CDV energy input was very low, but steel tube rupture was quite good. The magnitude of the pressure pulse caused by bubble formation was larger than in FAST 51 and 52. Other results were similar to those in FAST 51 and 52.

FAST 54. The water height was 710 mm for this test (as in FAST 51 through 53), but the xenon gas pressure in the fuel sample was five times less than that used in the previous three tests. Perhaps because of the reduced xenon pressure, the first bubble oscillation period was ~10 ms less than it was in FAST 51 through 53.

FAST 55. This was a water test, with the water height set to 1120 mm, in which pressure measurements were made in the argon gas and

under water (~230 mm from the test sample). A portion of the pressure data is shown in Fig. 1. Note that the maximum measured cover gas pressure occurred at roughly the same time as the minimum pressure measured underwater. This result makes us more confident that the maximum cover gas pressure occurs when the maximum bubble volume is produced.

FAST 56. This was a hot water test in which a high-speed movie (500 frames/s) was taken through the top vessel port. In a number of previous hot water tests,[2] aerosol measurements in the argon cover gas indicated that UO_2 had been transported through the water to the cover gas. We hoped that the movie results would indicate how this UO_2 transport occurred. Steel containment tube breakup was not efficient in this test, but UO_2 was again found in the cover gas after the test. Unfortunately, the movie did not provide clear evidence as to the means of aerosol transport; this test will be repeated at a later date.

Pressure data from measurements made in the cover gas (shown in Fig. 2) are quite encouraging. Not only was a measurable pressure change produced that is attributable to the initial bubble formation, but a secondary pressure event occurred that could perhaps be due to bubble reexpansion after first collapse. Because the transducer used has a 3.44-MPa pressure rating, both of the pressure signals are fairly small; however, if a unit with a lower rating can be used, larger (and hopefully more meaningful) data can be produced.

FAST 57. In this test two acoustic transducers were mounted on the vessel wall, one at the level of the test sample and the other ~160 mm above the test sample. The units were to be pulsed simultaneously, and "time-of-flight" data (the time for an acoustic pulse to be emitted, reflected from a surface, and collected by the transducer) were to be

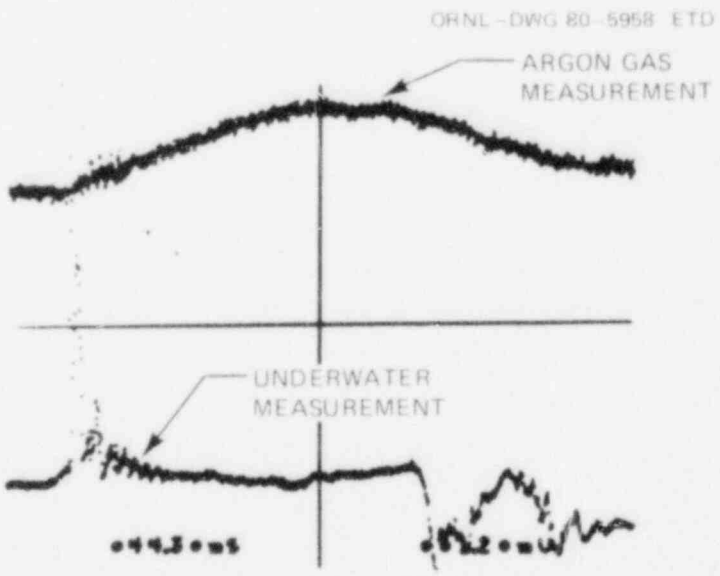

Fig. 1. Pressure data, measured in argon cover gas and underwater (~230 mm from test sample), in FAST 55. Note that peak argon gas pressure occurs roughly at the time of minimum measured underwater pressure.

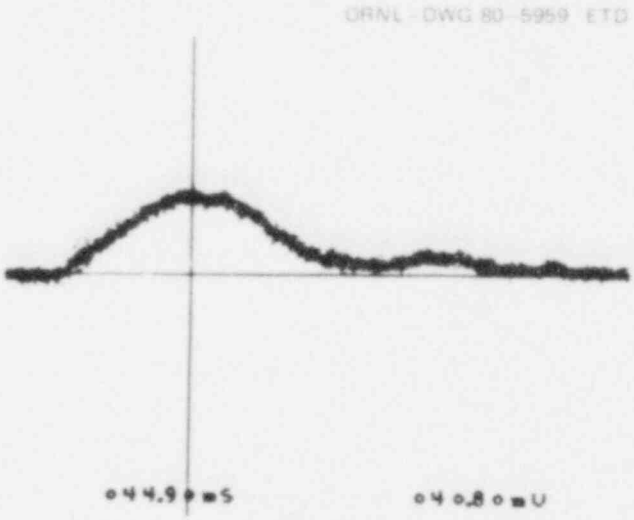

Fig. 2. Measured argon cover gas pressure vs time for FAST 56. Pressure maximum corresponding to 40.8 mV occurred 44.9 ms after start of capacitor discharge. Note second, much smaller, peak in argon gas pressure. (This could be caused by a second bubble oscillation.)

compared. During the test, CDV energy input was low and steel containment tube rupture was very poor. No meaningful data were obtained from the acoustic measurements; they seemed to indicate that there was no bubble produced in the test. This test will be repeated next quarter.

2.1.3 Discussion of results from CRI-III tests

Five tests were performed in the CRI-III facility this quarter. One was of the "energy density" type; the other four were related to the Sandia Normalization test series that began last year.[3,4] In particular, we were attempting to make measurements of fuel temperatures produced during preheat and capacitor discharge.

In addition to discussion of these tests, results are presented from CDV 97, 98, and 105, three "preheat-only" tests in which the samples were sectioned afterwards to permit pictures of sample cross sections to be made.

CDV 101. As will be discussed in detail later in this section, results from CDV 97 and 98 indicate full pellet melting is not being produced for the high preheat levels typically used in the capacitor discharge experiments. CDV 101 was an attempt to ensure that the pellets were molten at the start of capacitor discharge. A high preheat of 2100 W was used, 400 W greater than usually used for 90-mm-long samples. In addition, the cooling time between preheat and capacitor discharge was cut from 2 to 0.4 s, to suppress fuel cooling during this time. Capacitor discharge energy input was small, but aerosol measurements indicated that greater than a gram of aerosol was produced. George Parker participated in sampling the fuel aerosol, using cascade impactors connected in parallel.

CDV 102. As discussed in a previous quarterly report,[2] a new fuel viewing scheme is being attempted for the second series of Sandia Normalization experiments. The major purpose of the overall test series is to compare the fuel debris produced (at comparable UO_2 energy levels) by electrical energy input with that produced by neutronic energy input in Sandia's Annular Core Research Reactor (ACRR). Such a comparison requires measurement of fuel pellet temperatures caused by fuel heat-up. The fuel viewing scheme tried last quarter did not seem to work because of excessive shunting of current away from the exposed fuel pellet. The viewing set-up used in CDV 102 through 105, shown in Fig. 3, is similar to that tested last quarter except for one major difference. The number of layers of microspheres was varied between the exposed pellet and the view window. Hopefully, measurements can be made for varied microsphere packing layer thicknesses, and then an extrapolation can be performed to estimate the pellet temperature when the view window is absent.

CDV 102 was mainly performed to determine if there would be any problems associated with having a layer of micropsheres between the exposed pellet and view window. As expected, no problems were encountered with preheat and capacitor discharge.

CDV 103 (SN-8). R. M. Elrick and D. L. Fastle from Sandia Laboratories participated in CDV 103 through 105. As in the other normalization tests, the system pressure was maintained below ~100 μm Hg during the test. This was necessary in previous tests due to the debris sampling method used.[3] In CDV 103 through 105, movies were taken during fuel heat-up, and the fuel radiance that results in film exposure will be used to determine temperatures. No debris sampling was done in these tests.

In this test the exposed pellet had a 0.4-mm hole drilled to its center, and one layer of microspheres was between the pellet and view window. (The microspheres did not block the exposed hole.) Preheat and capacitor discharge went very well; the CDV energy input in this test was ~50%

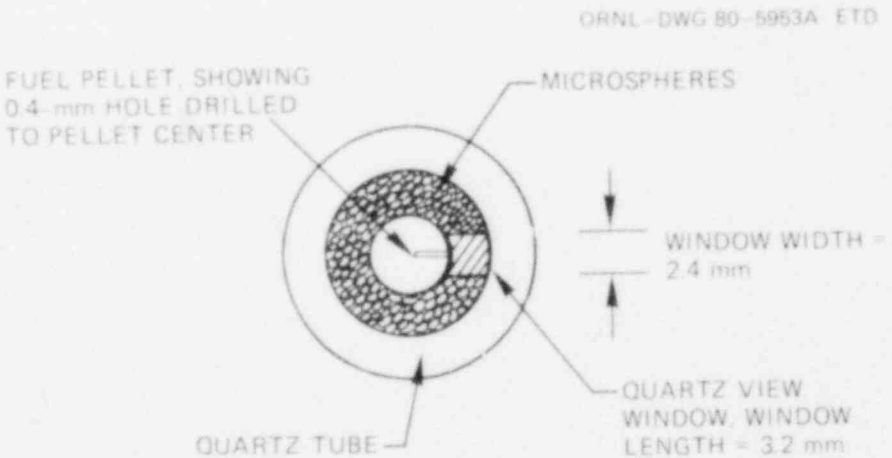

Fig. 3. Drawing of CDV sample cross section, illustrating "view window" installed in CDV tests 102 through 105. Number of microsphere layers between pellet and window was varied in these tests.

greater than in any of the previous normalization tests. Because of the reduced pressure in the vessel, the view windows were coated with UO_2 aerosol immediately after capacitor discharge.

CDV 104 (SN-9). In this test two layers of microspheres were put between the exposed fuel pellet and the view window. Capacitor discharge was somewhat shorter in CDV 104, but the current history up to the arcing time looked much like that for CDV 103.

CDV 105 (SN-10). This was a preheat-only test; the end of low preheat, the high preheat, and sample cool-down were filmed at 200 frames/s. The view window had one layer of microspheres between it and the exposed pellet. After the sample preheating was completed, the microsphere region near the window looked much different than the microspheres far from the window. This was probably the result of current shunting that occurred due to the presence of the view window in the sample. After the test the fuel sample was sectioned to photograph the condition of the fuel caused by the higher preheat.

Temperature determinations from the movies taken of CDV 103 through 105 should be completed next quarter.

Sample cross-section photographs from CDV 97, 98, and 105. The assumption has always been made that the preheat levels used in the CRI-III and FAST experiments produced near-to-total or total pellet melting. Recent calculations using newly developed preheat models (not yet documented in a report), however, seem to indicate that less of the pellets are melted than expected. CDV 97 and 98 were performed to permit us to learn what the melt fractions are for typical high-preheat levels. These were preheat-only tests: CDV 97, which had a 16-pellet stack (~110 mm long), was done with a 2200-W high preheat, while CDV 98, which had a 13-pellet stack (~90 mm long), was done with a 1700-W high preheat. These preheat levels are the ones typically used in capacitor discharge experiments, with the high preheat followed by the 2-s cooling time that immediately precedes capacitor discharge.

CDV 105 was another preheat-only test; it was performed as part of the Sandia Normalization test series (SN-10). We also decided to section this sample, particularly to look at the section of the sample where the view window was located.

Each quartz tube-UO_2 specimen was vacuum impregnated with epoxy and cut with a thin, water-cooled diamond abrasive wheel. The approximate locations of the cuts are shown in Fig. 4. Both faces at each of the five locations (e.g., faces labeled 1 and 2 in the diagram) were polished, and then photographs were taken of each polished surface. Photographs of faces 1, 2, 5, 6, 9, and 10 for each sample (CDV 97, 98, and 105) are shown in Figs. 5 through 13. For CDV 105, faces 5 and 6 coincided with the location of the quartz view window; a white mark shows the relative orientation of each photograph.

The following comments can be made related to Figs. 5 through 13.

1. The portion of each pellet shown in the pictures that became molten is that portion that became restructured and has a large-grained look. From the photos for CDV 97 and 98, about half of the pellets became molten.
2. Comparing CDV 98 and CDV 105, which were performed at the same 2200-W preheat level, more pellet melting occurred in CDV 105 than in CDV 97.

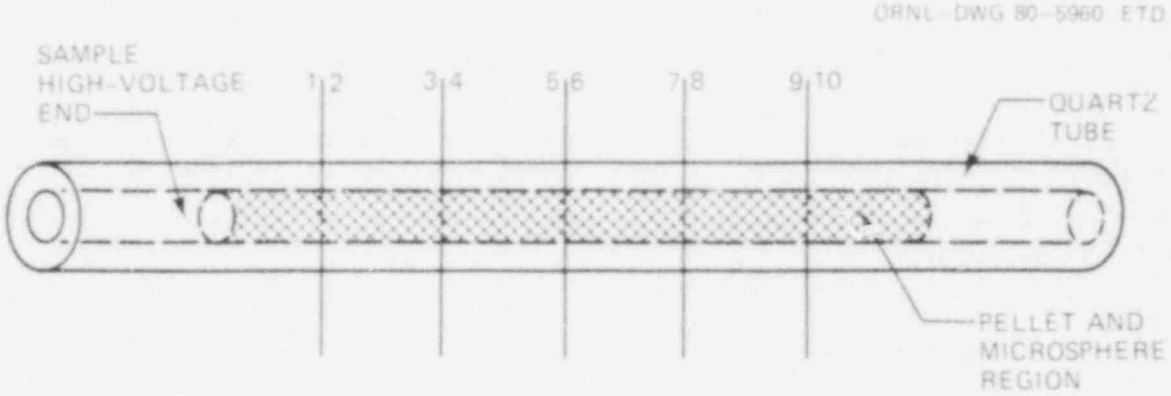

Fig. 4. Schematic of quartz-tube and UO_2 pellet-microsphere sample showing positions of five cuts made through samples for CDV tests 97, 98, and 105.

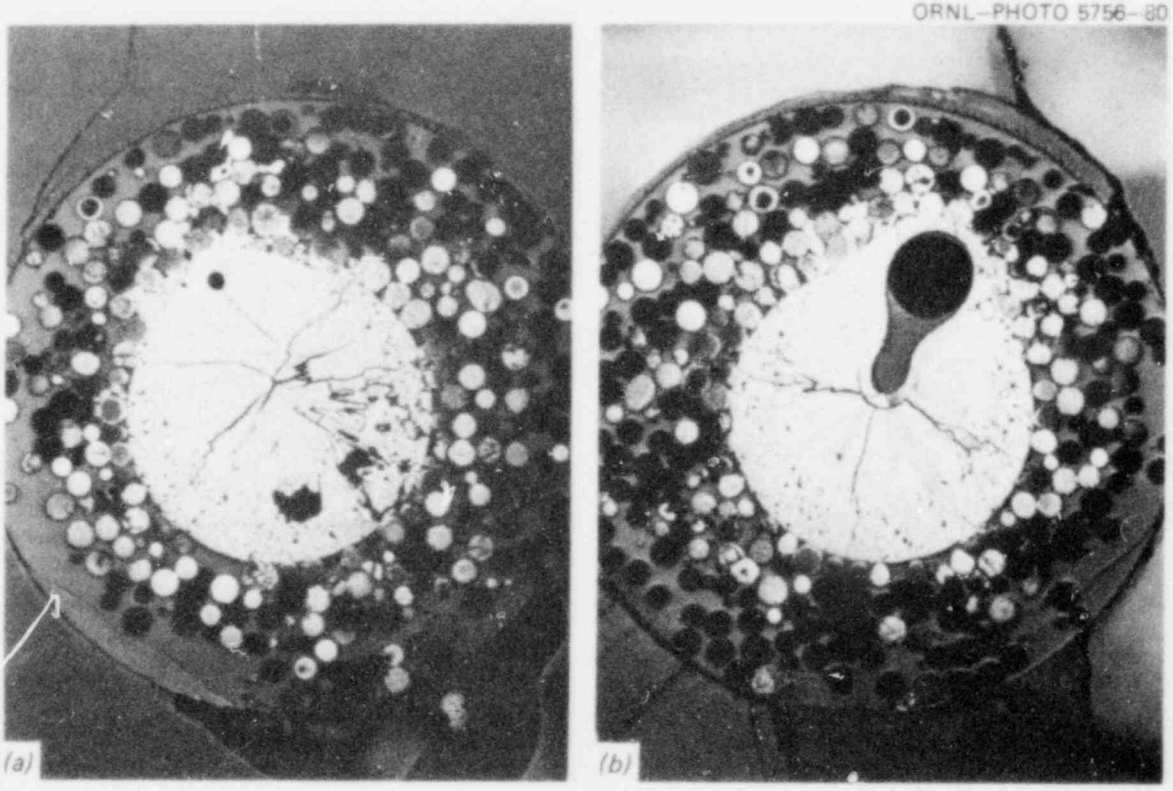

Fig. 5. CDV test 97 sample cross sections. (a) 97-1, (b) 97-2 (15×). (Original reduced 10%)

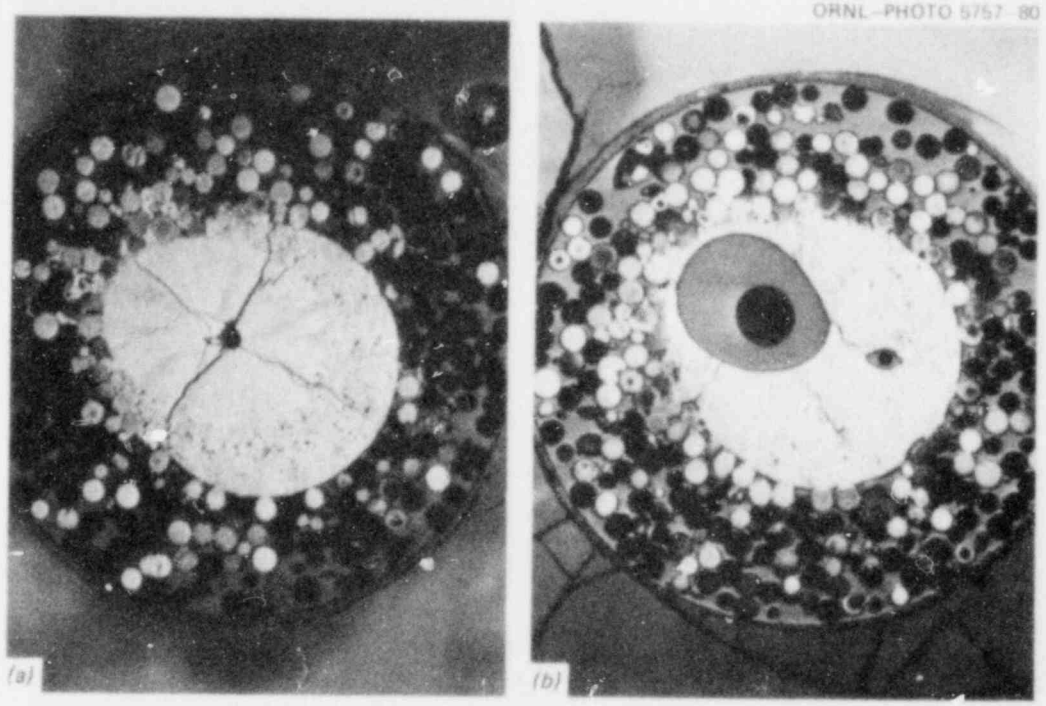

Fig. 6. CDV test 97 sample cross sections. (a) 97-5, (b) 97-6 (15×). (Original reduced 20%)

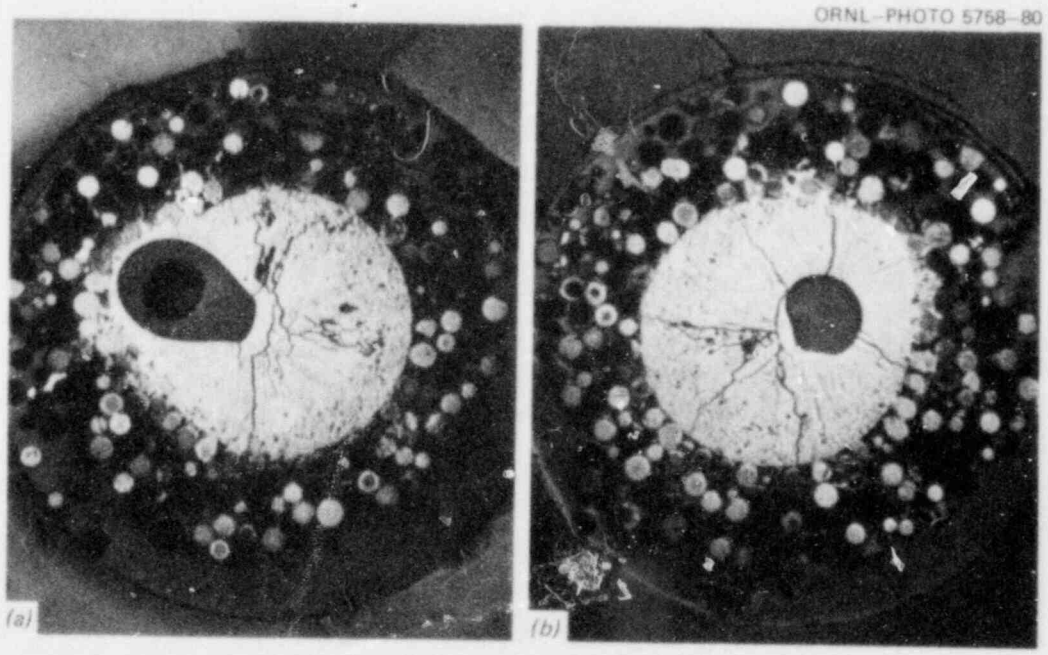

Fig. 7. CDV test 97 sample cross sections. (a) 97-9, (b) 97-10 (15×). (Original reduced 20%)

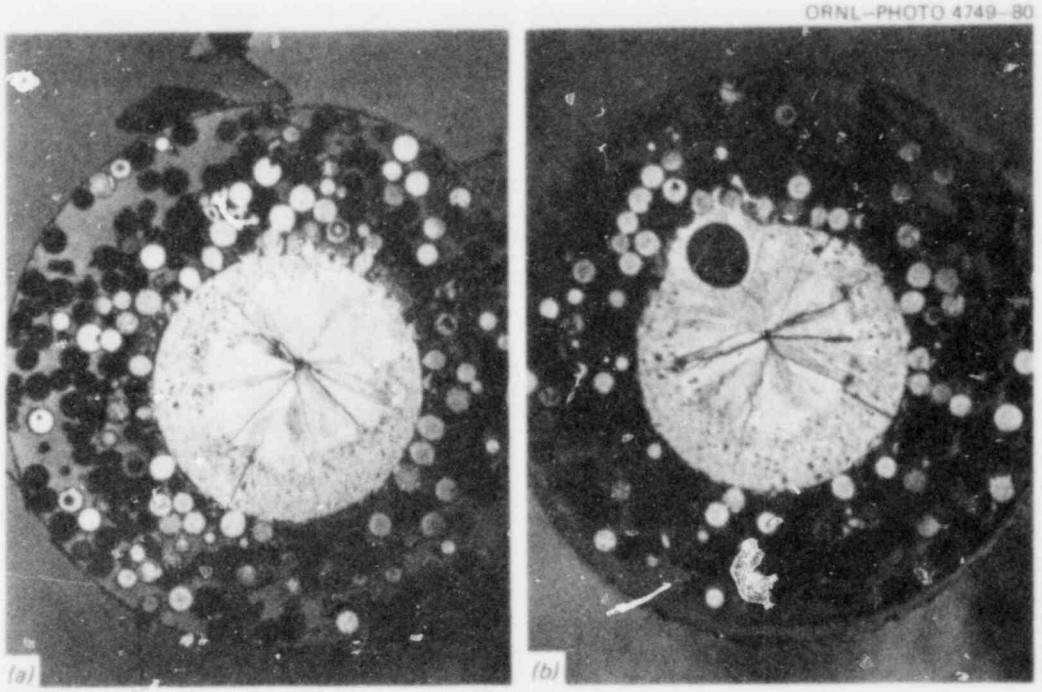

Fig. 8. CDV test 98 sample cross sections. (a) 98-1, (b) 98-2 (15×). (Original reduced 20%)

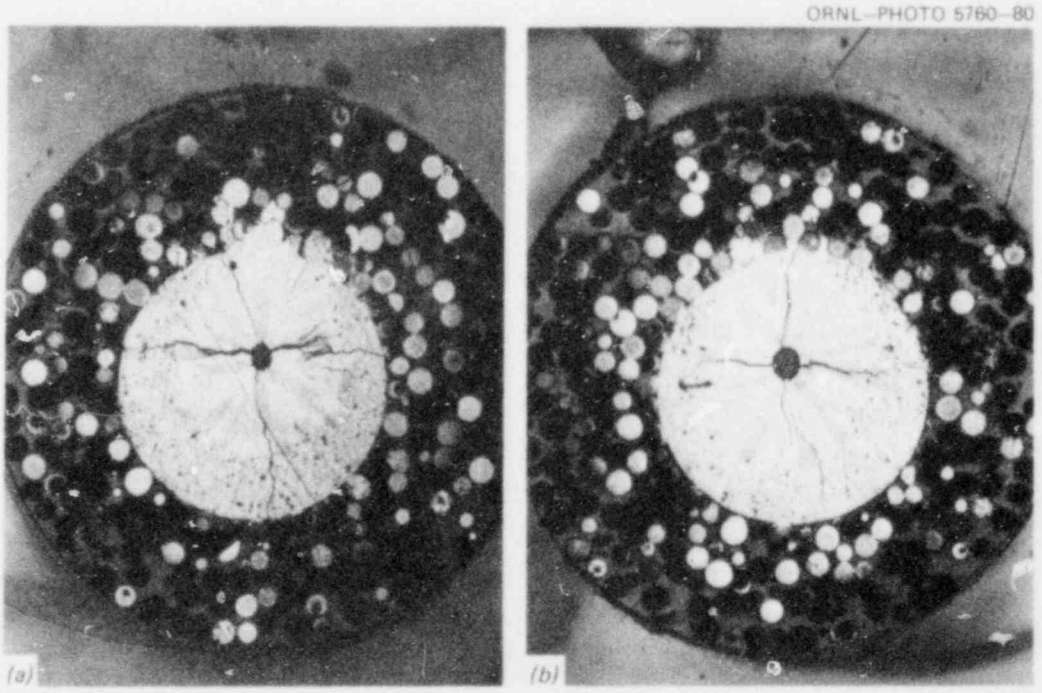

Fig. 9. CDV test 98 sample cross sections. (a) 98-5, (b) 98-6 (15×). (Original reduced 20%)

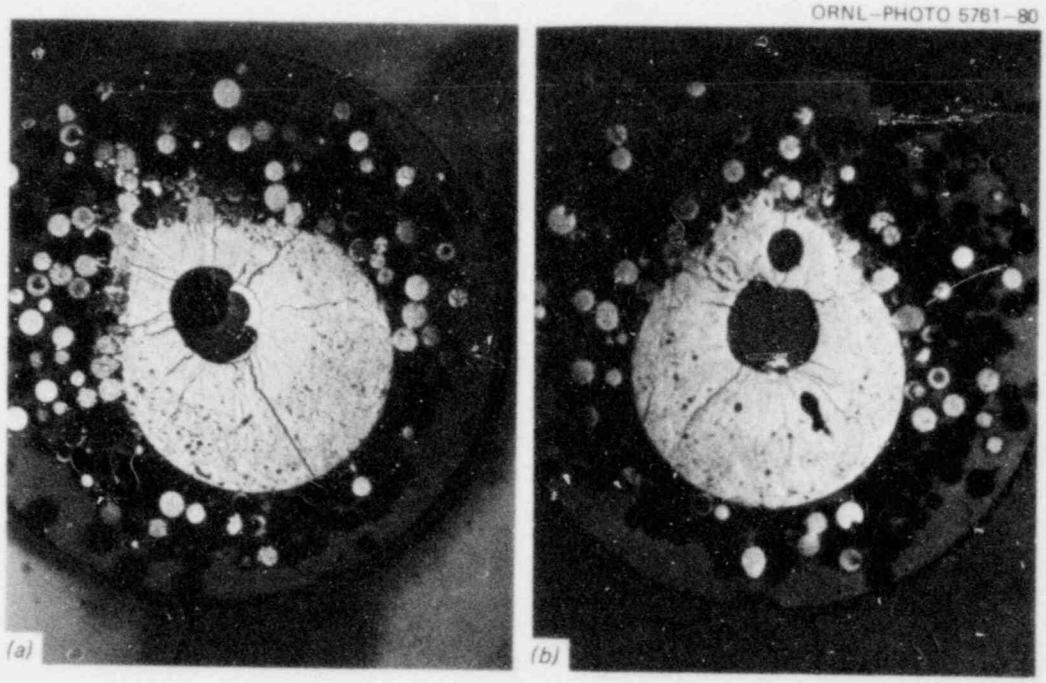

Fig. 10. CDV test 98 sample cross sections. (a) 98-9, (b) 98-10 (15×). (Original reduced 20%)

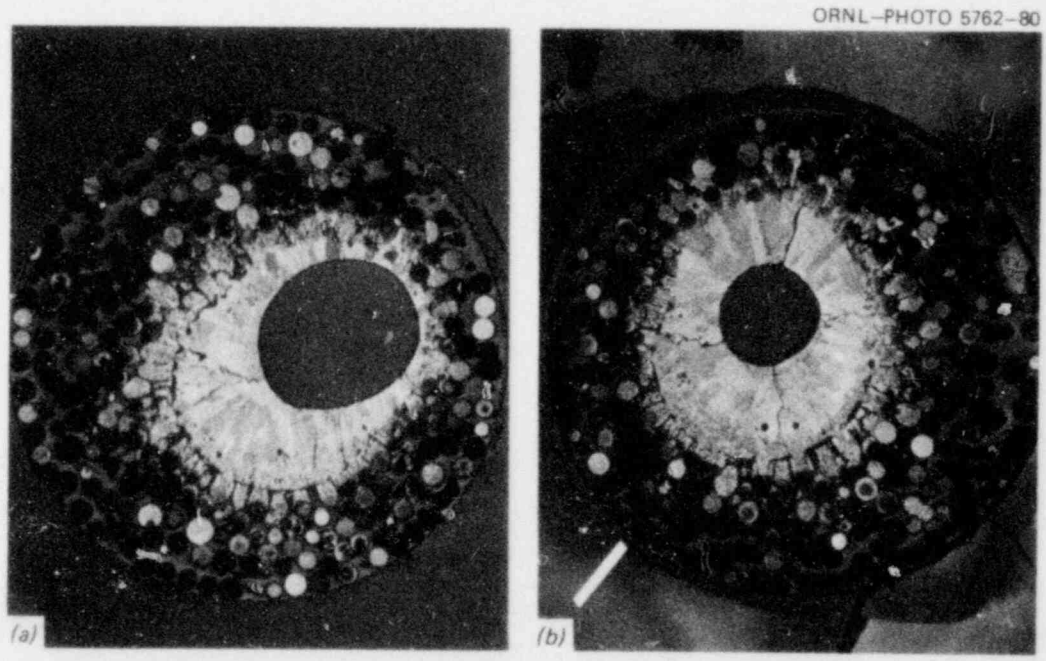

Fig. 11. CDV test 105 sample cross sections. (a) 105-1, (b) 105-2 (15×). (Original reduced 20%)

ORNL–PHOTO 5763–80

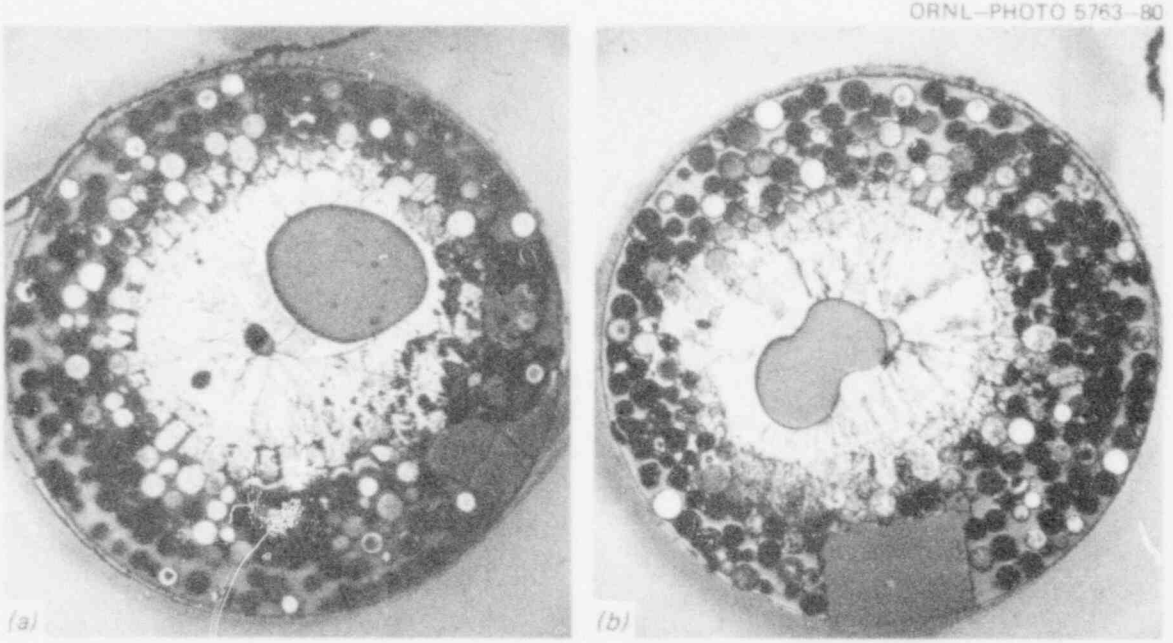

Fig. 12. CDV test 105 sample cross sections. (a) 105-5, (b) 105-6 (15×). (Original reduced 10%)

ORNL–PHOTO 5764–80

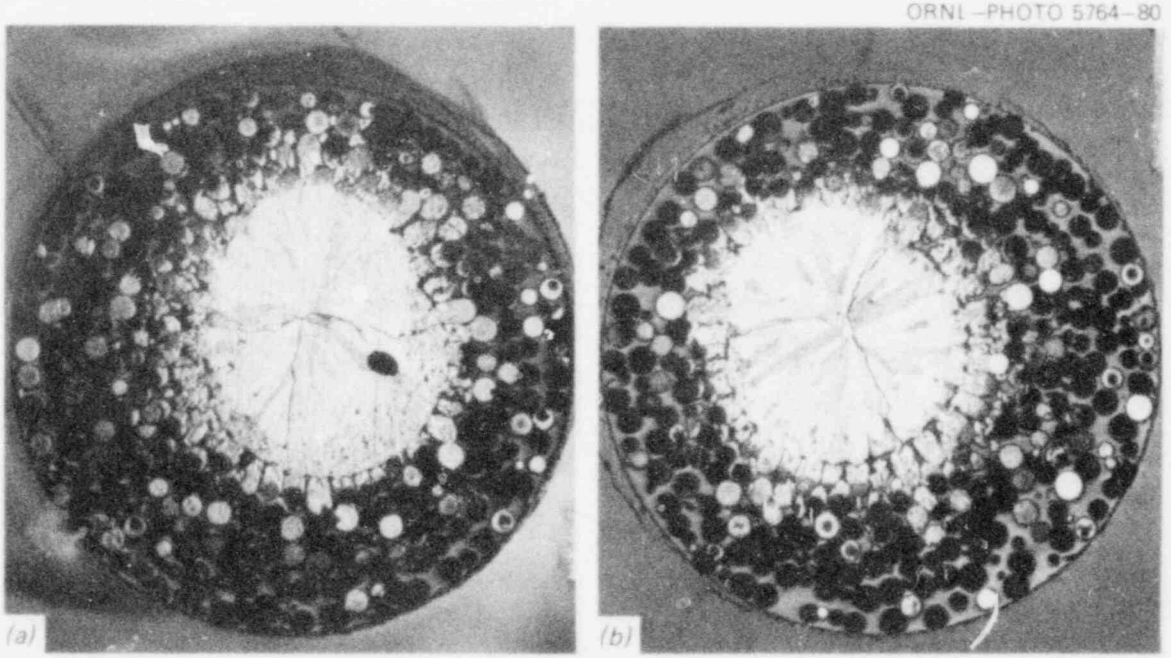

Fig. 13. CDV test 105 sample cross sections. (a) 105-9, (b) 105-10 (15×). (Original reduced 10%)

This may have been caused by the presence of the quartz view window in CDV 105.

3. When the melt front does not extend outside of the pellet radius, it seems to be circular. However, when it extends into the microsphere region, it takes on more of an ellipsoidal shape.
4. Voided regions in the melt are evident in some photographs. The largest voids seem to occur when the melt region extends into the microspheres.
5. Figure 12 shows a pellet section in the quartz view-window region for CDV 105. Comparing Figs. 11, 12, and 13, the presence of the view window seems to have very little influence on the orientation and extent of the melt front.

2.2 Secondary Containment Aerosol Studies in the NSPP

R. E. Adams

2.2.1 Introduction

Activities of the NSPP during the period included the performance of and analysis of data from a uranium oxide test under wet conditions (No. 208) and a low concentration sodium oxide aerosol test under dry conditions (No. 108).

2.2.2 Uranium oxide aerosol test No. 208

The purpose of this test was to investigate the effects of a highly humid atmosphere on the behavior of the U_3O_8 aerosol. The high humidity in the vessel atmosphere was produced by evaporating 11.4 L (3 gal) of water from the heated sodium burn pan over a period of about 100 min. Approximately 30 min after start of water boiling, the U_3O_8 aerosol generation was started and then continued for about 13.5 min; water evaporation continued for an additional 55 min after termination of aerosol generation.

The most noticeable effect of the high humidity on the aerosol was a change in physical appearance. Electron photomicrographs showed the aerosol to be in the form of nearly spherical agglomerates as contrasted with the chain-like agglomerates normally found in previous tests under dry conditions.

Aerosol mass concentration. An average maximum aerosol concentration of 12.5 $\mu g/cm^3$ was measured about 0.5 min after termination of aerosol generation. Aerosol mass concentration as a function of time is given in Fig. 14. While the physical form of the agglomerates was changed by the presence of moisture, the aerodynamic behavior of the wet aerosol was not very different from that of the dry aerosols. For example, in the dry aerosol tests (205 through 207), the time required for the maximum aerosol concentration to be reduced by a factor of 10 varied from 90 to 125 min; for this wet U_3O_8 test, the time required was 100 min.

Aerosol particle size. The aerodynamic mass median diameter of the aerosol was measured with cascade impactors (Andersen Mark III) over the

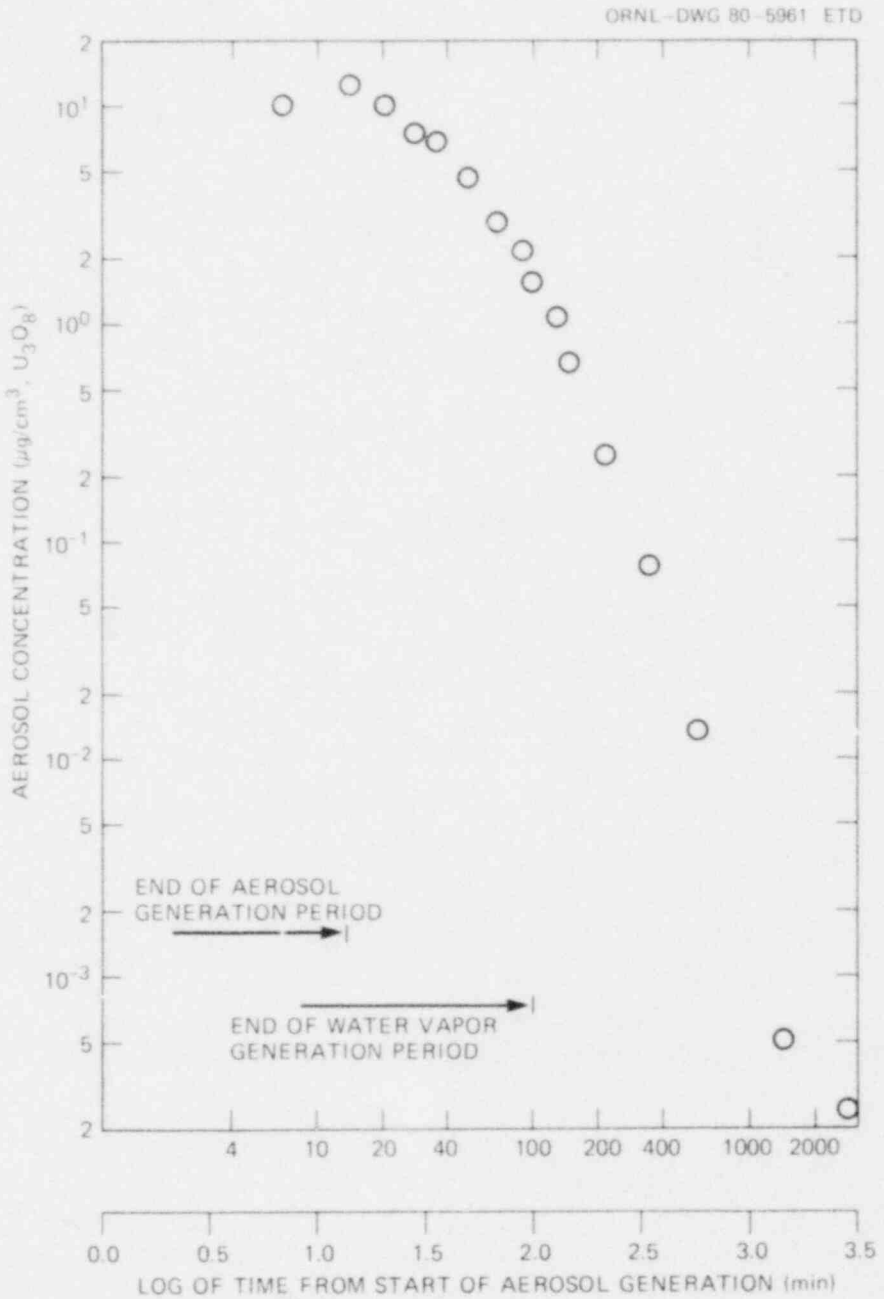

Fig. 14. Average aerosol mass concentration (test 208).

first 24 h of the test. The results are listed in Table 4. Sample 7 contained a sufficient quantity of uranium oxide for analysis; however, the distribution deviated signficantly from log normal and a mass median diameter could not be determined.

Aerosol distribution. At the termination of the test (48 h), the approximate aerosol distribution, as determined by the fallout and plate-out samplers and the final filter sample, was as follows: aerosol settled

Table 4. Uranium oxide aerosol particle size — test 208

Sample No.	Time (min)	AMMD[a] (μm)	σ_g[b]
1	26.3	3.3	1.7
2	59	3.8	1.6
3	111	4.4	1.5
4	223	4.6	1.6
5	348	5.8	1.7
6	583	5.4	2.4
7	1471	c	c

[a]Aerodynamic mass median diameter.

[b]Geometric standard deviation.

[c]For explanation, see Sect. 2.2.2 of text.

onto floor of the vessel, 87%; aerosol plated onto internal surfaces, 13%; and aerosol still suspended in the vessel atmosphere, 0.002%.

2.2.3 Sodium oxide aerosol test No. 108

The purpose of this test was to study the behavior of a low concentration sodium oxide aerosol under dry conditions. This test completed the planned series of tests on sodium oxide aerosols. The aerosol was generated by a sodium pool fire of 0.45 kg (1 lb) of heated sodium metal. The vessel atmosphere was air at a relative humidity of less than 20%, and the initial temperature and pressure were slightly above ambient because of the preheating of the sodium burn pan and delivery line. Test duration was 48 h.

Aerosol mass concentration. The aerosol was generated over a 2- to 2.5-min period, and a maximum aerosol concentration of 2.25 μg/cm^3 was measured at 10 min after initiation of the pool fire. Aerosol mass concentration as a function of time is given in Fig. 15. The rate of disappearance of this aerosol was slower than those observed previously for sodium oxide aerosols in the 6 to 25 μg/cm^3 range. For example, in the higher concentration tests (101 through 104), the time required for the maximum aerosol concentration to be reduced by a factor of 10 varied from 90 to 100 min; for this test, the time required was about 200 min.

Aerosol particle size. Cascade impactor measurements were made over the first 24 h of the test. Results are given in Table 5. The aerodynamic mass median diameters for this low concentration aerosol was not greatly different from those measured during the higher concentration sodium oxide tests.

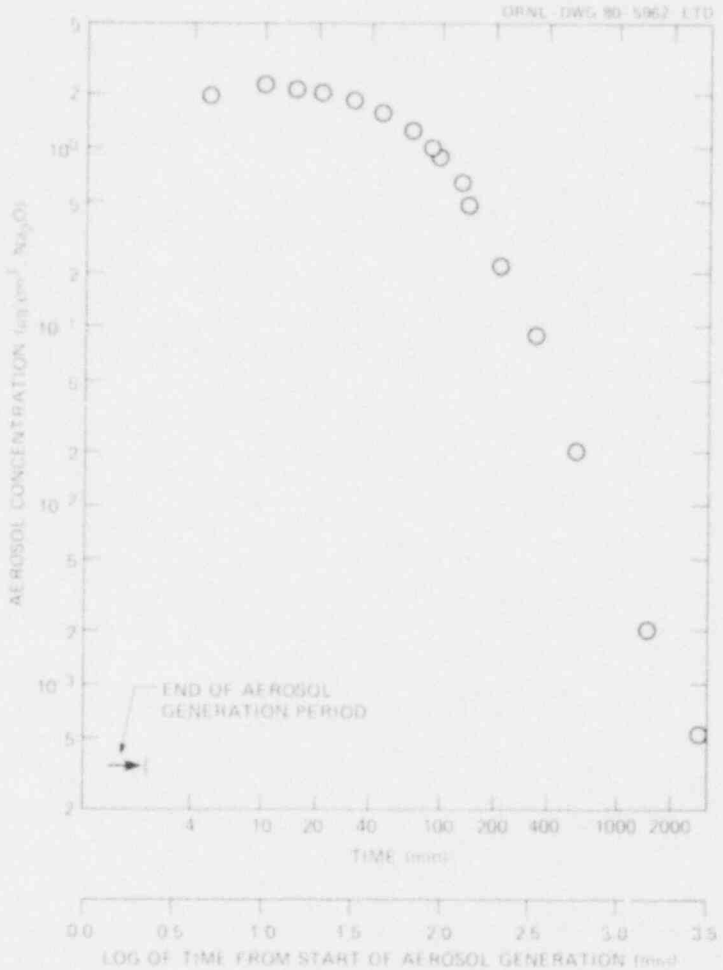

Fig. 15. Average aerosol mass concentration (test 108).

Table 5. Uranium oxide aerosol particle size -- test 108[a]

Sample No.	Time (min)	AMMD (µm)	σ_g[b]
1	23.5	3.0	1.7
2	56.6	4.1	1.8
3	111.4	3.8	1.7
4	231	3.4	1.6
5	350	2.9	1.6
6	596	1.6	1.9
7	1445	1.5	1.7

[a] Aerodynamic mass median diameter.

[b] Geometric standard deviation.

Aerosol distribution. At the termination of the test (48 h), the approximate aerosol distribution, as measured by the fallout and plateout samplers and the final filter samples, was as follows: aerosol settled onto floor of the vessel, 60%; aerosol plated onto internal surfaces, 40%; aerosol still suspended in the vessel atmosphere, less than 0.03%.

2.3 Basic Aerosol Experiments in CRI-II

George Parker A. L. Sutton, Jr.
George Creek

2.3.1 Introduction

In previous quarterly progress reports we have presented various data on size measurements of high-density aerosols of uranium oxides (U_3O_8 and UO_2), sodium peroxide (Na_2O_2), and mixed oxides of U_3O_8 and Na_2O_2.

During early investigations a single cascade impactor, the Andersen Mark II, was found to give fairly consistent results which could be closely approximated by the calculated sizes based on settling velocities. At least two other instruments that required a very high gas velocity through a small jet were indicating much smaller agglomerate sizes; in fact, they gave a nearly constant size distribution while the low-velocity impactor was more correctly indicating increasingly larger sizes in proportion to increasing initial concentrations. The conclusion has since been made that the high velocity jets were fragmenting the chain agglomerate particles.

Later, as more varied size measuring instruments were obtained and applied to the task, a relatively constant and reproducible series of measurements were made by each. Then the introduction of the LASL-Stöber spiral centrifuge finally provided a very readily calibrated instrument, which in turn gave unequaled reproducibility and therefore much greater precision. Lower geometric standard deviations were also observed in the centrifuge measurements, which further supports the conclusion that all inertial jet impactors tend to fragment particles to some extent causing a wider range of size distributions.

2.3.2 Comparison of size measurements performed by means of the spiral centrifuge with various impactors

Since initiating the comparative study to evaluate the quality of size measurements obtainable from several commercial impactors, testing a series of these instruments in parallel with the spiral centrifuge and then comparing the results in terms of aerodynamic mean mass diameter and geometric standard deviation for a given aerosol at a given time in its deposition cycle has been relatively simple. The collected impactor plates are shown in Fig. 16, and the results are summarized in Fig. 17. Additional measurements are compared in Table 6. The relative uniformity of deposition behavior of several aerosol tests in CRI-II is illustrated in Fig. 18 for U_3O_8, Na_2O_2, and for one mixed oxide run. The U_3O_8 and Na_2O_2 runs were of nearly the same initial mass concentration, and these

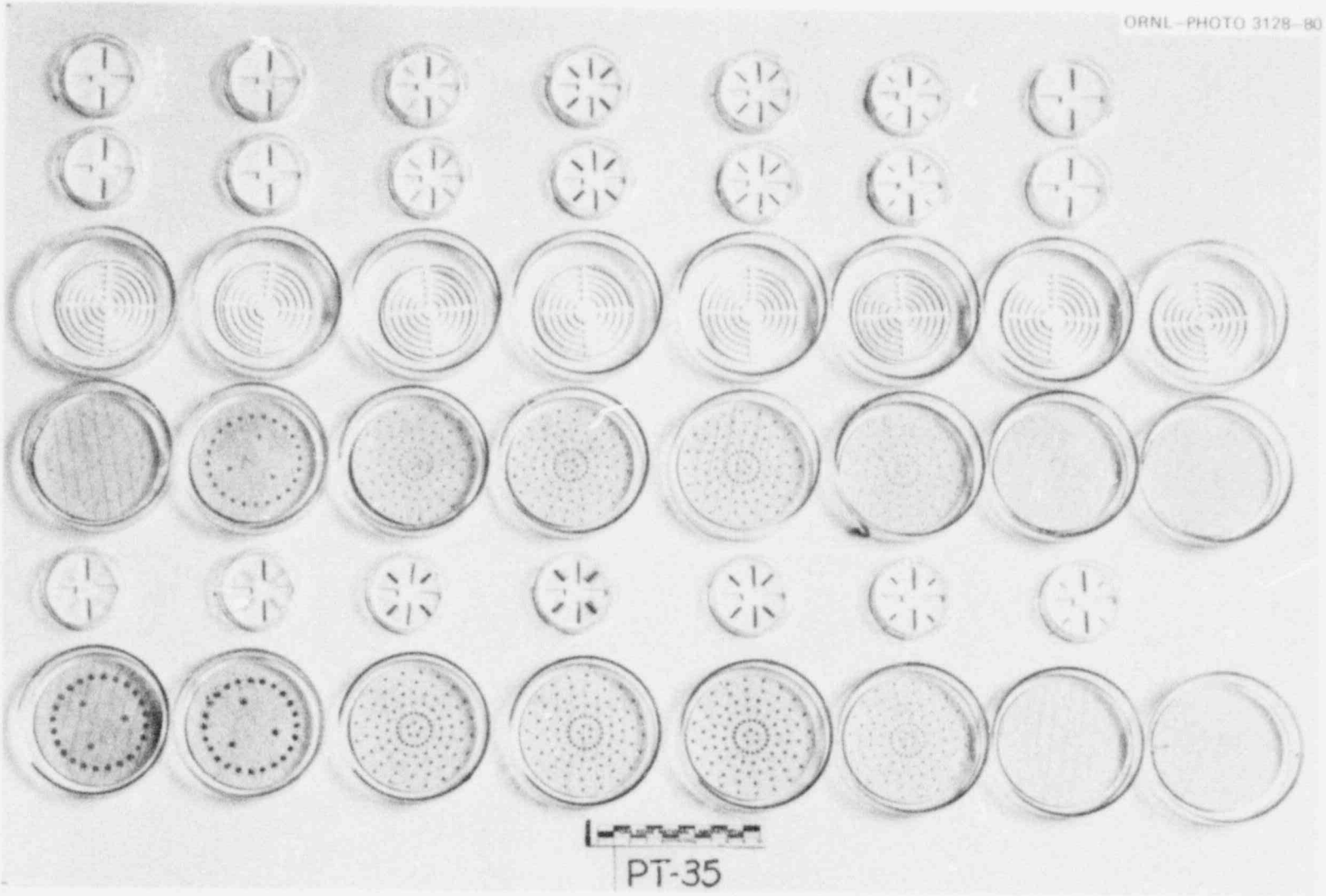

Fig. 16. Typical impactor collector plates with U_3O_8 aerosol for Andersen Mark II, Mark III, and Sierra Impactors.

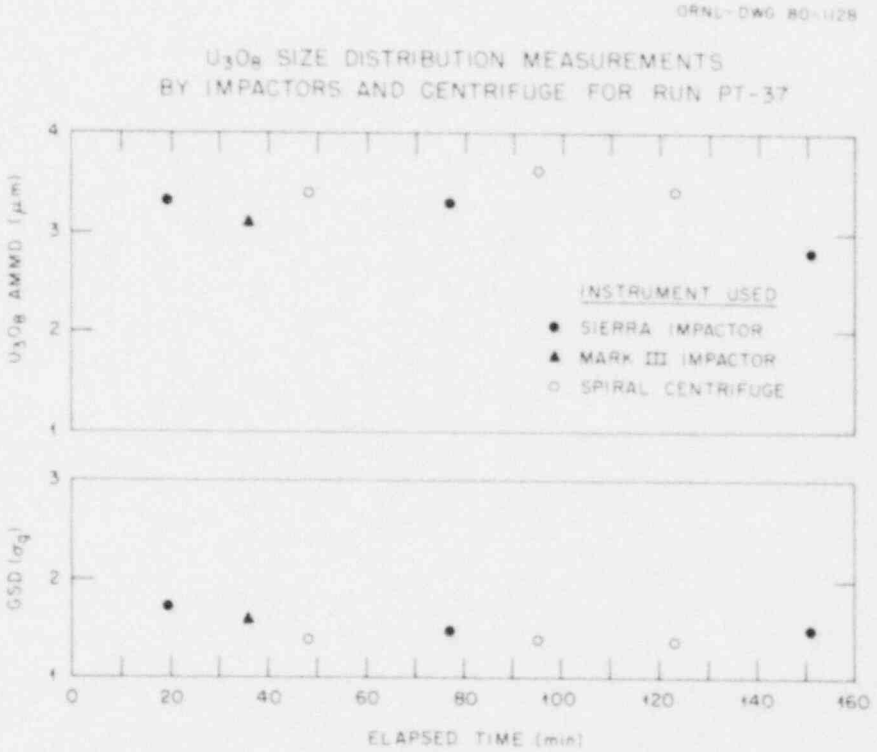

Fig. 17. Comparison of size distribution measurements for centrifuge and various impactors.

Table 6. Comparison of size distribution measurements for the centrifuge and various impactors

	Sampling time (min)		AMMD[a] (μ)	σ_g[b] (μ)
	From	To		
Sierra impactor	19	20	3.66	1.72
Andersen impactor (+ preseparator)	25	27	2.23	2.52
Mark III impactor	35	37	3.11	1.57
Spiral centrifuge	43	53	3.39	1.38
Sierra impactor	76	79	3.31	1.47
Spiral centrifuge	82	107	3.61	1.41
Andersen impactor	116	126	2.43	1.57
Sierra impactor	147	157	2.76	1.51
Spiral centrifuge	193	253	3.41	1.37

[a] Aerodynamic mass median diameter.

[b] Geometric standard deviation.

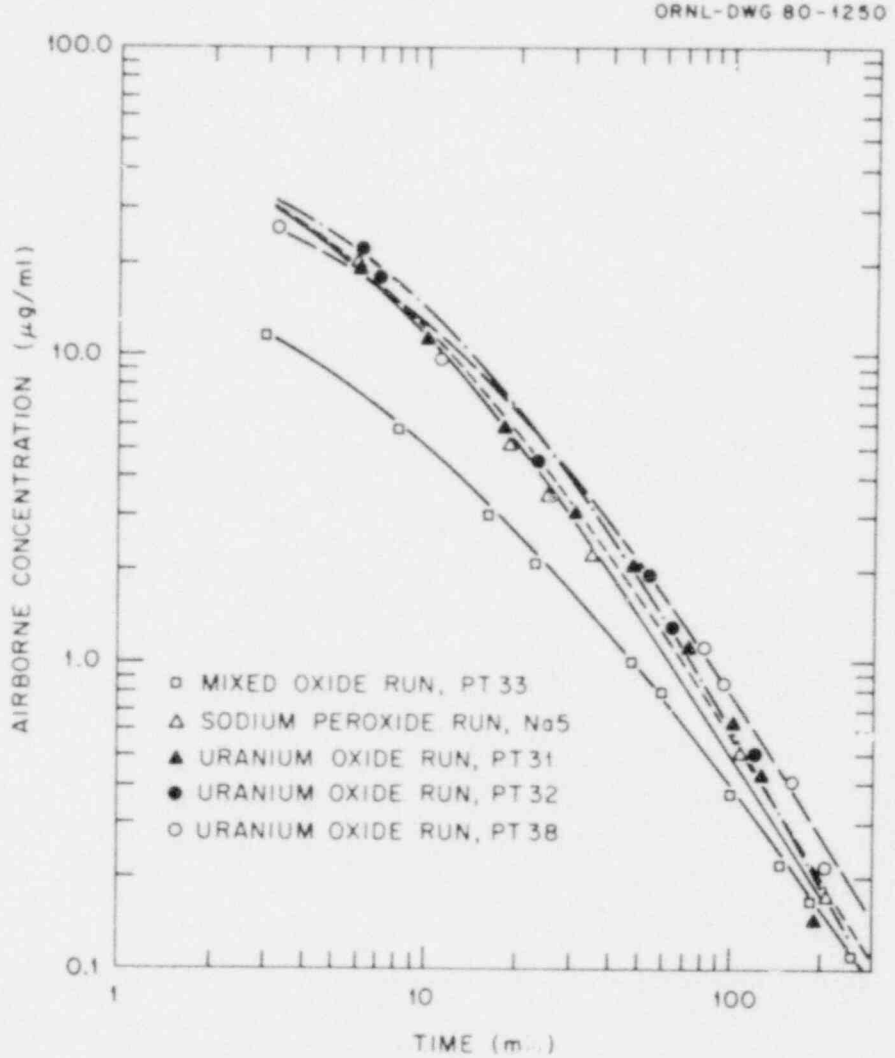

Fig. 18. Rate of deposition of sodium peroxide and uranium oxide in CRI-II.

were all very closely matched in deposition rate. The single mixed oxide run, in which a significantly lower concentration was generated, showed a much lower deposition rate, as expected. A set of sample photomicrographs of a sodium peroxide aerosol is shown in Fig. 19, and a set of sample photomicrographs of separated U_3O_8 particles from the centrifuge in Fig. 20.

2.3.3 Intercomparison of aerosol size test data with other laboratories

A systematic review of all fuel and sodium aerosol measurement data readily available from the current literature and from all ongoing NRC and Department of Energy reactor safety programs was attempted some time ago and has gradually been nearing completion. Results of the review are

ORNL-DWG 80-1222

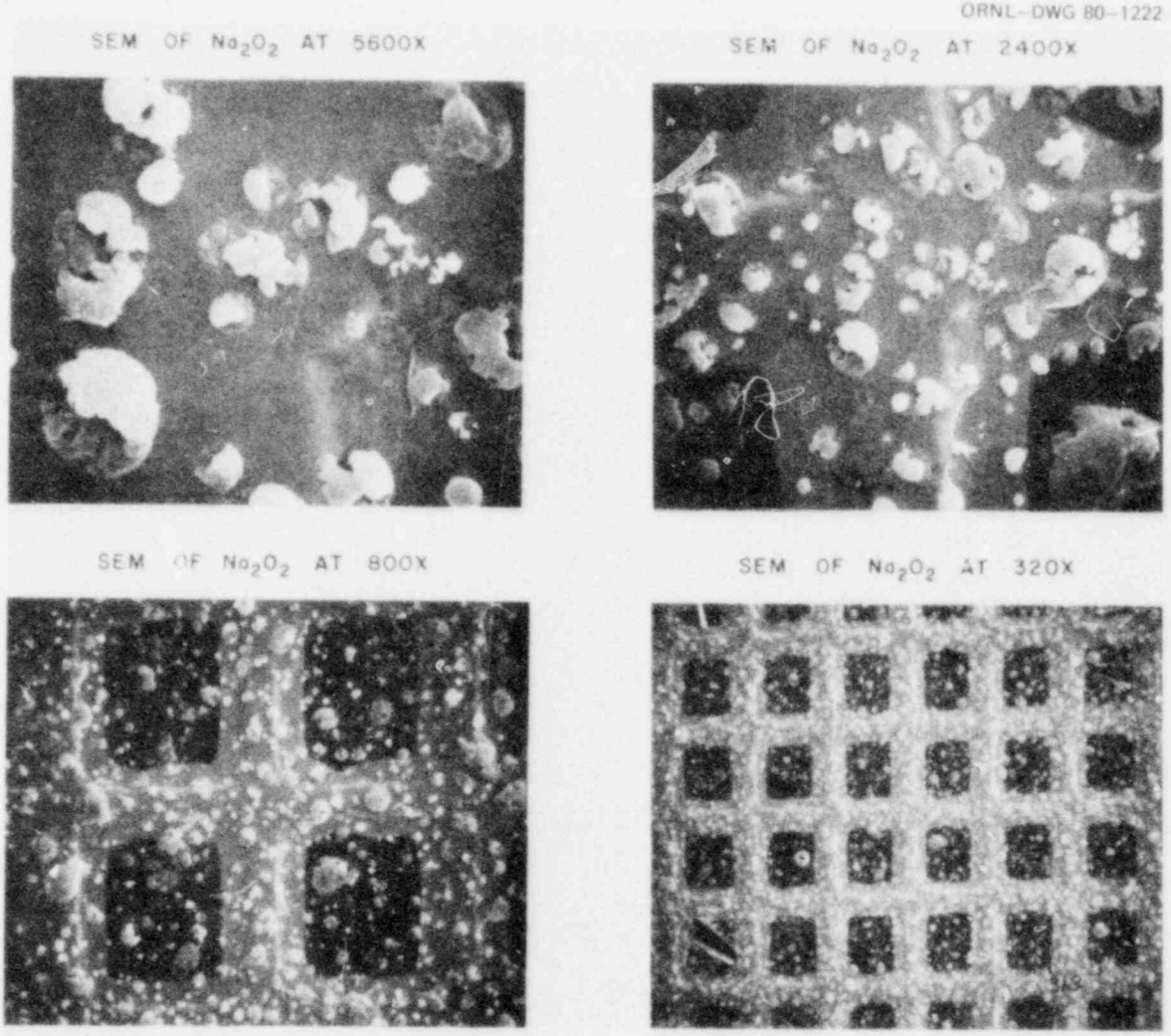

Fig. 19. Typical Na_2O_2 particles as seen by scanning electron microscopy. (Original reduced 21%)

listed in Tables 7 and 8 in which comparisons within the fuel aerosol category are made in one and within the sodium oxide aerosol category in the other.

The range of results is relatively wide; however, for the most part they are consistent with the assessed accuracy of the measuring instrument and vary in proportion to the mass concentration being measured. Slightly higher mean sizes seem to be observed at a constant mass concentration when measured in the larger containment facilities like the ORNL NSPP and the Hanford Containment Systems Test Facility (CSTF), suggesting that there may be a small positive containment vessel height effect on the maximum agglomerated particle diameter measured.

The most obvious conclusion to be drawn from this study is that all of the low-velocity commercial-sized measuring instruments are capable of giving good qualitative size distributions; however, precision measurement can only be made with an aerosol mass spectrometer (i.e., the centrifuge).

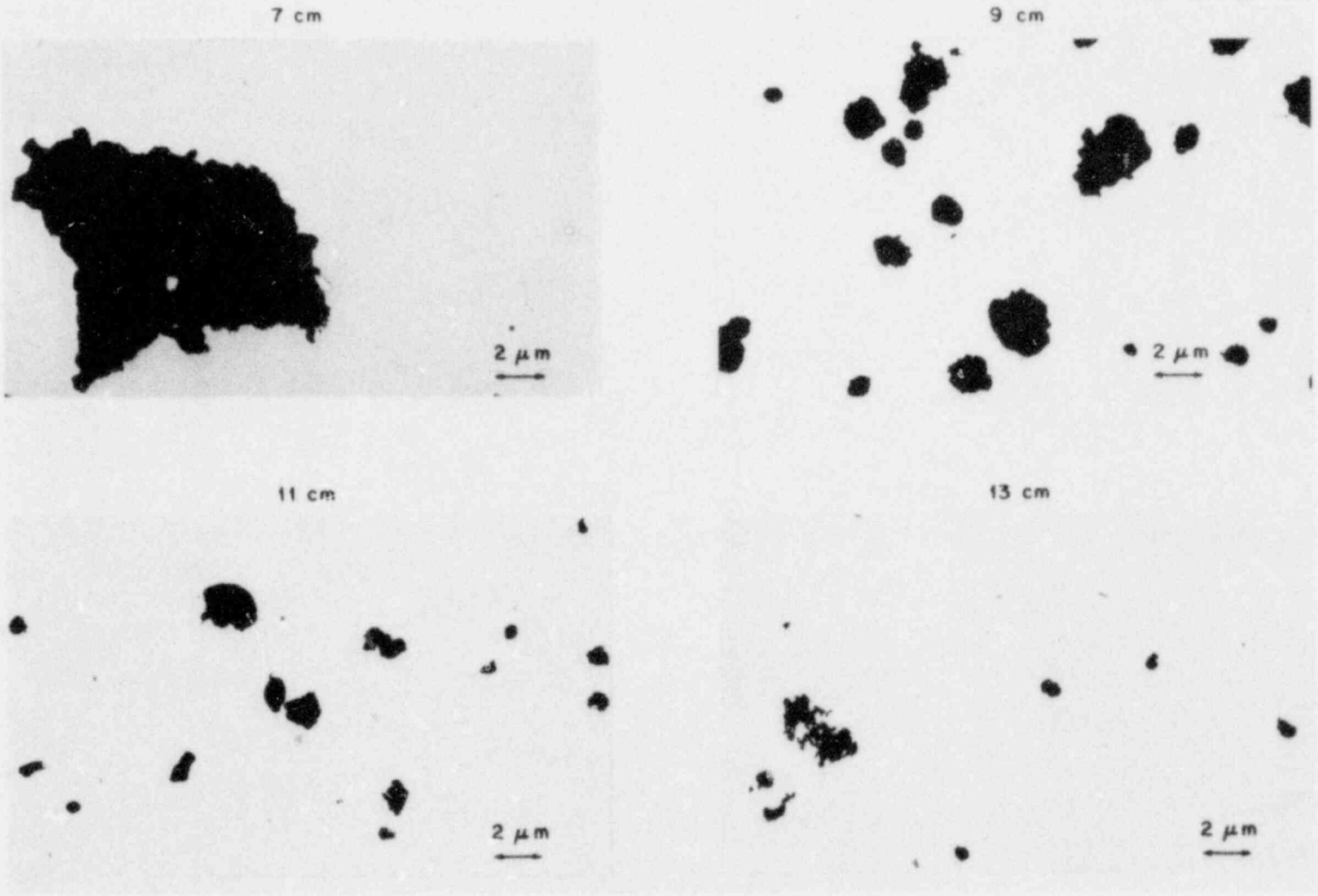

Fig. 20. Typical U_3O_8 particles deposited at selected intervals on the spiral centrifuge foil. (Original reduced 11%)

Table 7. Size measuring devices used in sodium aerosol technology

Laboratory	Investigator	Instrument type	Manufacturer or identification	Instrument range, AMMD	AMMD found (μm)	Estimated accuracy (%)	Additional information derived
ORNL (NSPP)	R. E. Adams, T. S. Kress	Impactor C(8)	Andersen samplers	0.5–13	7.0	±20	σ_g = 2.7 at 6.0 g/m^3
Harvard (School of Public Health)	W. Hinds	Concentric centrifuge	M. I. Tillery, LASL	1.0–5.0	1.85	±5	σ_g = 1.65 at 3.0 g/m^3 Effective density = 0.61
		Impactor C(8)[a]	Andersen samplers	0.4–11	3.5–4.0	±20	σ_g = 2.0 at 10 g/m^3
HEDL (CSTF)	R. K. Hilliard, J. D. McCormack et al.	Impactor C(8) Mark III	Andersen samplers	0.5–13	6.4	±10	σ_g = 2.66 at 30 g/m^3
		Impactor R(8)	Sierra Insts.	0.9–18		±10	Calibration being corrected
Rockwell International (A.I.-STV)	H. A. Morewitz, C. T. Nelson, M. Silberberg	Impactor C(4)	Lovelace (modified)	0.1–2.2		±20	
		Impactor C(8)	Andersen (N.V.)	0.4–11	5.5	±20	σ_g = ? at 30 g/m^3
		Impactor C(5)	Andersen (mini)				
SUNY[b] (Buffalo)	D. T. Shaw, J. Wegrzyn	Impactor C(8)	Advanced Sciences	0.5–16			
		Impactor C(7)	Lovelace Laboratory	0.5–20			Effective density
		Impactor R(4)[c]	Cassella-May	0.1–5		5–30	Error increases with size
		Centrifuge	Stöber Spiral	0.1–6.0		±5	Bimodal distribution of forms
ORNL (CRI-II)	G. W. Parker et al.	Impactor C(8) Centrifuge	Andersen MK-II LASL-Stöber	0.5–11	4.3	±15	σ_g = 1.8 at 30 g/m^3
		Na_2O_2		0.5–12	3.7	±5	σ_g = 1.4 at 30 g/m^3
		Mixed oxide		0.5–12	5.1	±5	σ_g = 1.5 at 40 g/m^3

[a] C = circular jet impactor (number stands for number of stages).

[b] State University of New York.

[c] R = rectangular jet impactor (number stands for number of stages).

Table 8. Size measuring devices used in uranium oxide aerosol technology

Laboratory	Investigator	Instrument type	Manufacturer or identification	Instrument range, AMMD	AMMD found (μm)	Estimated accuracy (%)	Additional information derived
ORNL (NSPP)	R. E. Adams et al. (1976–1979)	Impactor C(8) Mark III	Andersen samplers	0.5–11	1.7	±15	σ_g = 2.7 at 6 g/m^3
Rockwell International A.I.	H. A. Morewitz, C. T. Nelson, R. P. Johnson (1966–1978)	Impactor C(5) Elutriator[a]	Andersen (mini) A.I.	0.1–4.7		±15 NA	
ORNL (CRI-II)	G. W. Parker	Impactor R(8)	Sierra 2110	0.5–18	3.5	±15	σ_g = 1.8 at 30 g/m^3
		Impactor C(6)[b]	Andersen samplers	0.7–11	2.4	±15	σ_g = 2.5 at 1 g/m^3
		Impactor C(8)[c]	Andersen samplers	0.5–11	3.5	±15	σ_g = 2.0 at 30 g/m^3
		Spiral centrifuge	LASL-Stöber	0.5–20	4.0	±5	σ_g = 1.4 at 30 g/m^3
ORNL (CRI-III-CDV)	M. J. Kelly, A. P. Wright	Impactor C(6)	Andersen samplers	0.7–11	3.0	±15	σ_g = 2.2 at 6 g/m^3
		Impactor C(6)L[c]	H. Bucholtz[c]	0.01–3.5			
BNL	A. W. Castleman	T.E.M. and settling rates	NA	(For PuO_2)	0.9–1.2	NA	σ_g = 1.6 at 0.3 g/m^3
				(For UO_2)	0.6–1.6	NA	σ_g = 1.8 at 0.3 g/m^3

[a]The elutriator is a special settling chamber being developed for high temperature size measurement.

[b]All high velocity jet devices such as inertial impactors tend to fragment long-chain agglomerated aerosols, typical of UO_2, U_3O_8, and PuO_2.

[c]The low pressure impactor has been found to be useful mainly with unagglomerated particles or as a backup in tandem extension of the ambient impactors.

3. ANALYTICAL PROGRAM

M. L. Tobias

3.1 Improved Formulas for Bubble-Liquid Interface Temperatures for FAST Experiment Analysis

The previous quarterly progress report discussed a formula for the temperature at a bubble-liquid interface through which heat was flowing:

$$T(0,t) - T_\infty = \frac{1}{k}\sqrt{\frac{4}{\pi}\, q\, \bar{q}\, \alpha\, t}\ , \tag{1}$$

where $T(0,t)$ and T_∞ are the temperatures at the interface and an "infinite" distance into the liquid, respectively, k is the thermal conductivity, q is the instantaneous heat flux at time t, $\bar{q}$ is the time-averaged value of the heat flux up to time t, α is the thermal diffusivity of the liquid medium. This formula was developed by modifying a result obtained using the integral balance method. While it is exact for slab geometry and q constant in time, it suffers from inaccuracy in certain situations. For instance, if $q = 0$ at some time, Eq. (1) predicts the incorrect result $T(0,t) = T_\infty$.

The exact solution referred to above for slab geometry is[5]

$$T(0,t) - T_\infty = \frac{1}{k}\sqrt{\frac{4\alpha t}{\pi}}\left[\int_0^t \frac{q(t-\tau)\,d\tau}{\sqrt{t\tau}}\right]. \tag{2}$$

If $q(t)$ is linear in time, then the bracketed expression may be written in terms of $\bar{q}$ and the value at t as

$$\left[\ \right] = \frac{2}{3}\bar{q} + \frac{1}{3}q\ . \tag{3}$$

If $q(t)$ is parabolic in time, then the bracketed expression becomes

$$\left[\ \right] = \frac{4}{5}\bar{q} + \frac{4}{15}q - \frac{1}{15}q(0)\ , \tag{4}$$

where $q(0)$ is the heat flux at time 0.

Both expressions have the virtue that they will not break down if $q = 0$. Use of the linear formula with the parabolic heat source used above produces the following comparison.

Time	Exact factor	$2/3\ \bar{q} + 1/3\ q$	Difference (%)
0	7000	7000	0.0
0.5	4901	4910	0.2
1.0	3266	3305	1.2
1.5	2100	2187	4.1
2.0	1400	1555	[illegible]

[The use of $(4/5)\ \bar{q} + (4/15)\ q - 1/15\ q(0)$ will of course produce exact agreement with the analytical result.]

Although the formula in Eq. (4) is often much closer to the exact solution than the "linear" formula [Eq. (3)], it can give negative results if q is a rapidly decreasing function of time. This is easily seen by using a broken line function for q, that is, $q = a - bt$ for $0 \leq t \leq a/b$, and $q = 0$ for $t \geq a/b$. For long enough times, the $-1/15\ q(0)$ term will cause Eq. (4) to give negative results. A comparison of two cases shows this effect for t = 2s.

	$q = 7{,}000 - 7{,}000t$, $0 \leq t \leq 1$; $q = 0 (t \geq 1)$	$q = 7{,}000 - 70{,}000t$, $0 \leq t \leq 0.1$; $q = 0$, $t \geq 0.1$
Exact result	967.	88.3
Linear formula [Eq. (3)]	1,167. (21%)	116.7 (32%)
Parabolic formula [Eq. (4)]	933. [illegible]5%)	−326.7 (−470%)

The figures in parentheses are the percentage deviations of the approximation results from the exact answers.

While the linear formula [Eq. (3)] is not of the highest accuracy, it cannot produce negative results and so will not lead to unphysical answers. Using it appears to be the best compromise for analysis of FAST underwater tests.

The above studies suggest the idea of representing q by a series of broken line functions in Eq. (2), obtaining as close an approximation to the analytical answer as one pleased. Unfortunately, such a technique is not recursive and would produce a very long running code because of the need to update each term of the resulting series as the time t changed.

3.2 Programming Efforts in Support of the NSPP Experimental Program

Attention has been given to making the computer processing of NSPP data more efficient. This has involved some changes in the five programs usually used as well as in the way they are implemented. Recent changes in the central programming system have made it possible to eliminate the use of punched cards almost entirely in favor of CRT-equipped typewriter terminals.

REFERENCES

1. A. L. Wright and A. M. Smith, *Updated Work Plan for the FAST/CRI-III Fuel Vaporization and Transport Experiments*, ORNL/NUREG/TM-326 (October 1979).

2. T. S. Kress and M. L. Tobias, *LMFBR Aerosol Release and Transport Program Quarterly Progress Report for January–March 1980*, ORNL/NUREG/TM-416, to be published.

3. T. S. Kress and J. T. Han, *LMFBR Aerosol Release and Transport Program Quarterly Progress Report for January–March 1979*, ORNL/NUREG/TM-329 (August 1979).

4. T. S. Kress and A. L. Wright, *LMFBR Aerosol Release and Transport Program Quarterly Progress Report for April–June 1979*, ORNL/NUREG/TM-354 (January 1980).

5. H. C. Carslaw and J. C. Jaeger, *Conduction of Heat in Solids*, 1st Edition, Oxford University Press (1948), p. 57.

NUREG/CR-1791
ORNL/NUREG/TM-417
Dist. Category R7

Internal Distribution

1. R. E. Adams
2. M. Bender
3. H. W. Bertini
4. J. R. Buchanan
5. W. B. Cottrell
6. G. F. Flanagan
7. M. H. Fontana
8. U. Gat
9. H. W. Hoffman
10-14. T. S. Kress
15. R. E. MacPherson
16. A. P. Malinauskas
17. F. R. Mynatt
18. G. W. Parker
19. P. Patriarca
20-21. J. L. Rich
22. J. M. Rochelle
23. A. M. Smith
24. I. Spiewak
25. A. L. Sutton, Jr.
26. D. G. Thomas
27-29. M. L. Tobias
30. H. E. Trammell
31. D. B. Trauger
32. J. L. Wantland
33. J. A. Stevens
34. R. P. Wichner
35. G. D. Whitman
36. A. L. Wright
37. ORNL Patent Office
38. Central Research Library
39. Y-12 Document Reference Section
40-41. Laboratory Records Department
42. Laboratory Records (RC)

External Distribution

43. M. Silberberg, Chief, Experimental Fast Reactor Safety Research Branch, Division of Reactor Safety Research, Nuclear Regulatory Commission, Washington, DC 20555
44. D. L. Basdekas, Division of Reactor Safety Research, Nuclear Regulatory Commission, Washington, DC 20555
45. R. Sherry, Division of Reactor Safety Research, Nuclear Regulatory Commission, Washington, DC 20555
46-49. Director, Office of Nuclear Regulatory Research, Nuclear Regulatory Commission, Washington, DC 20555
50. Office of Assistant Manager for Energy Research and Development, DOE, Oak Ridge Operations Office, Oak Ridge, TN 37830
51-52. Technical Information Center, DOE, Oak Ridge, TN 37830
53-432. Given distribution as shown in category R7 (NTIS-10)

☆U.S. GOVERNMENT PRINTING OFFICE: 1980-640-245/411